

# Quantitative nanoparticle structures from ultrafast electron crystallography data

Christopher L. Farrow

Department of Applied Physics and Applied Mathematics, Columbia University,  
New York, NY, 10027, USA

Chong-Yu Ruan Department of Physics and Astronomy, Michigan State University,  
East Lansing, MI, 48824, USA

Simon J. L. Billinge

Department of Applied Physics and Applied Mathematics, Columbia University,  
New York, NY, 10027, USA

Condensed Matter Physics and Materials Science Department,  
Brookhaven National Laboratory, Upton, NY 11973  
sb2896@columbia.edu

## Abstract

We describe the quantitative refinement of nanoparticle structures from gold nanoparticles probed by ultrafast electron crystallography (UEC). We establish the equivalence between the modified radial distribution function employed in UEC and the atomic pair distribution function (PDF) used in x-ray and neutron powder diffraction analysis. By leveraging PDF refinement techniques, we demonstrate that UEC data are of sufficient quality to differentiate between cuboctahedral, decahedral and icosahedral nanoparticle models. Furthermore, we identify the signatures of systematic errors that may occur during data reduction and show that atomic positions refined from UEC are robust to these errors. This work serves as a foundation for reliable quantitative structural analysis of time-resolved laser-excited nanoparticle states.

## 1 Introduction

Ultrafast electron crystallography (UEC) is a promising new approach for studying the structure of photoexcited materials on pico and femtosecond timescales.[1, 2] It extends existing ultrafast pump-probe spectroscopy techniques by providing vital structural information on the photoexcited states, which is required to obtain a more complete understanding of these transient states. It has long been a dream to make “molecular movies” [3, 4, 5] of atoms as a material transforms from one state to another. The use of x-rays for this purpose, obtained from powerful synchrotron sources and in the future from hard x-ray free electron lasers, has the advantage that the data can be modeled quantitatively using existing x-ray crystallographic[6] and atomic pair distribution function[7] (PDF) approaches. However, on the experimental side, the use of electrons as a probe has a number of advantages over synchrotron x-ray techniques. First, the scattering power of the electrons is higher, allowing smaller and more dilute samples to be studied. Second, it is easier to control the pulse

structure of the probe-pulse on femtosecond time-scales without the need for fast choppers.[8]

A challenge when using electrons as a probe is that the scattering is strong, resulting in increased multiple scattering, and the single-scattering kinematical approximation used in most x-ray analyses may not be valid. Recent developments in quantitative electron crystallography,[9] especially with the development of precession methods of data collection,[10] show that these problems can be overcome under certain circumstances and quantitative structure solutions are possible using electrons. Another challenge is structure solution when the underlying structural correlations only extend over nanometer dimensions, the so-called “nanostructure problem”.[11] Here we explore whether methods developed for quantitative structure solution[12] and refinement[13, 14, 15] of x-ray or neutron derived PDFs can be extended to UEC data from nanoparticles. The full potential of UEC can be realized only when the quantitative reliability of structures determined from the data is established. We investigate this issue here for the case of data from metallic nanoparticles tethered to a surface.

There is a large literature on the structure solution of small molecules in the gas phase from electron diffraction data.[16] However, the UEC experiments of interest are on samples in the solid or liquid phase where the validity of the kinematical approximation is less clear. Quantitative structure solutions from electron crystallography based on kinematic scattering are possible using very thin crystals,[17, 18] weakly scattering specimens[19, 20] and nanoparticles containing just 10-20 unit cells.[21] In these cases, the probability of a multiple-scattering event is sufficiently small that it can be treated as a minor perturbation on the single-scattering signal, and the data can be properly corrected for a quantitative structure solution.[22] Here we investigate whether UEC data from nanoparticles tethered to a surface can be treated in this way. There are powerful tools emerging for the study of nano-scale structures from ensembles of nanoparticles using x-ray and neutron diffraction data.[11, 12, 23, 24, 25, 26] These tools can also be applied and extended for studying UEC data if the quantitative reliability of the data in the kinematical limit can be established.

In this paper we show that it is possible to obtain UEC data of sufficient quality for quantitative structure modeling. We investigate the robustness of structural solutions with respect to uncontrolled aspects of the data reduction such as the use of empirical methods for removing incoherent backgrounds and determining an effective electron-form-factor that considers the absorption by the substrate. We elucidate potential sources of error in the data reduction procedure, and indicate the signature those errors. Additionally, we show the relationship between the correlation functions traditionally used in gas-phase electron diffraction, and those used in the study of nanostructure with x-rays and neutrons, bringing together these two fields of study. These results place the UEC method on a more sound footing with respect to the study of ensembles of nanoparticles, opening the door to reliable quantitative structure solution of transient states, and therefore physically meaningful molecular movies of these materials.

## 2 UEC with nanoparticles

The photochemical processes of bond breaking and forming can be resolved using femtosecond laser techniques in a pump-probe configuration, in which the first laser pulse (pump) is used as a trigger to initiate the chemical reactions and the ensuing probe laser pulse serves to monitor the changes via spectroscopic responses.[3] By replacing the probe laser pulse with a laser-triggered ultrashort electron pulse, the transient structural dynamics can be directly probed. This ultrafast electron diffraction (UED)[27] method was shown to be especially advantageous in the studies of optically dark processes, such as nonequilibrium structural transformation,[28] and radiationless relaxation channels for the photo-excited state.[29]

The UEC development extends UED to the condensed phase, and has been applied to study the collected excitations involving photons, electrons and phonons from the interfacial water bilayers and superconductors.[30, 31, 32] Whereas the periodic orders from the crystalline samples offer higher signal-to-noise ratio (SNR), and potentially, higher spatiotemporal resolutions, the complexity of the

anisotropic scattering in the dynamical scattering regime poses significant challenges in quantitatively assessing all the possible details of the relevant atomic dynamics that the higher SNR can now provide.

Recently, UEC has been applied to investigate nanoparticles that are highly dispersed on a surface to produce powder-like patterns for size-scale down to 20 Å.[2] To suppress the background signals from the supporting substrate, soft-anchoring of the nanoparticles using self-assembled molecular (SAM) layer on silicon surface is employed. The implementation of this specific UEC for studying nanoparticles (as shown in Fig. 1) affords a low coverage to ensure the scattering from isolated particles can be recorded unobstructively, and provides the needed chemical and physical isolation of nanoparticles under repetitive time-resolved studies.[33]

Even though a relatively clean coherent diffraction pattern for nanoparticles can be obtained this way by rendering the scattering from the substrate largely diffusive, it is still unclear how the residual effects caused by the uncontrolled diffusive background and the surface absorption affect the quantitative retrieval of structural functions. The empirically derived structural functions from UEC[33] will be refined using standard x-ray PDF analysis to examine the self-consistency and robustness of UEC data for quantitative structural analysis.

### 3 Correlation functions

In this section we discuss the relationship between the modified radial distribution function (mRDF) obtained from UEC experiments with the PDF obtained from x-ray and neutron measurements. Historically, the mRDF has been applied in gas-phase electron diffraction to study atom-pair correlations in small molecules containing a few to tens of atoms. In UEC, the mRDF is used to study the change in atomic arrangements in excited-state bulk- and nanostructures.[2, 34]

The mRDF,  $R(r)$ , is defined as the truncated Fourier transform of the molecular scattering

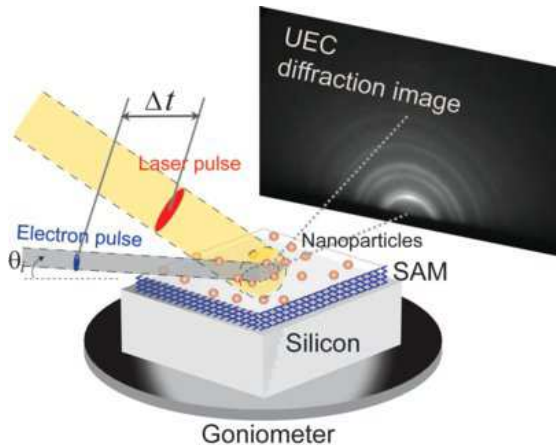


Figure 1: UEC for nanoparticles experimental setup, implementing the laser-pump-electron-probe configuration. The electron pulse is delayed relative to the 'pumping' laser pulse in a time-sequence ( $\Delta t$ ) to examine the structural dynamics. The incident angle of the electron beam is kept low, typically 1-2°, to achieve high sensitivity to the nanoparticles, which are dispersed on a self-assembled molecular monolayer atop a supporting silicon substrate, to produce powder-like diffraction patterns.

intensity,[35]

$$R(r) = \int_0^{s_{max}} sM(s) \sin(sr) \, ds, \quad (1)$$

where  $s$  is the magnitude of the scattering momentum transfer and  $s_{max}$  is the maximum determined value of  $s$ . The molecular scattering intensity,  $M(s)$ , contains the structural information extracted from the scattered electron intensity. The mRDF and  $sM(s)$  contain the same structural information, and it is the  $sM(s)$  curve that is typically used in structural modeling.[36, 16]

The PDF,  $G(r)$ , is used in x-ray and neutron investigations of liquids, and amorphous and nanostructured materials.[7] The PDF is the truncated Fourier transform of the reduced total scattering structure function,  $F(Q)$ .[37]

$$G(r) = \frac{2}{\pi} \int_{Q_{min}}^{Q_{max}} F(Q) \sin(Qr) \, dQ, \quad (2)$$

where  $Q$  is the magnitude of the scattering momentum transfer[38] and  $Q_{min}$  and  $Q_{max}$  are the measured  $Q$ -extrema. For elastic scattering,  $Q = (4\pi/\lambda) \sin(\theta)$ , where  $\lambda$  is the wavelength of the probe, and  $2\theta$  is the scattering angle. Note, the scattering angle in the gas phase electron diffraction literature is generally denoted  $\theta$ , rather than  $2\theta$ . Notation aside,  $Q$  and  $s$  are equivalent:

$$Q \equiv s. \quad (3)$$

In deference to the respective literatures, and to help differentiate between the two sets of functions, we will use  $s$  when referring to UEC and  $Q$  in reference to x-ray and neutron diffraction.

As we will show in the next section,  $F(Q)$  and  $sM(s)$  are effectively the same, where the only differences come about due to experimental effects and uncertainties in the data reduction process. These being equal, the important difference between the mRDF and PDF is the lower integration limit in their respective definitions.[37]

There is always a finite lower bound on the measured scattering momentum ( $s$  or  $Q$ ) due to experiment geometry and physical limitations of measure-

ment equipment. It is the practice in gas-phase electron diffraction and UEC to compensate for this missing scattering intensity by using a presumed structural model.[35, 2] In gas-phase electron diffraction the missing intensity below  $s_{min}$  is extrapolated to  $s = 0$  using the model, and in UEC the same effect is achieved by adding a baseline to the transformed real-space signal. This works well when the system under study is made up of individual small molecules in a dilute gas phase. However, it becomes highly problematic in condensed systems. In this case, the convention in x-ray and neutron diffraction is to ignore any scattering in the low- $Q$  limit.

When the Fourier transform includes the intensity extending to  $s = Q = 0$ , one obtains the mRDF, which is always positive (apart from termination effects due to a finite  $s_{max}$ ). However, if the small angle scattering is excluded, one obtains the PDF, which is a function that oscillates around zero, sitting on top of a negative baseline.[37] In either case, with the same minimum and maximum momentum transfer, the same structural information can be obtained from the mRDF or the PDF. We use the PDF in this study in order to avoid the extra step of compensating for the missing scattering information.

## 4 Data reduction in detail

In this section we will describe how  $sM(s)$  is obtained in practice in order to examine the systematic errors that may affect the extraction of structural information from the data. We will first discuss how the total scattering structure function is typically obtained in x-ray and neutron diffraction. This process has an established theoretical foundation,[7] and will serve as a basis of comparison with the UEC data reduction procedure.

### 4.1 X-ray and neutron diffraction data reduction

The reduced total scattering structure function,  $F(Q)$ , is defined in terms of the total scattering structure function,  $S(Q)$ , as  $F(Q) = Q(S(Q) - 1)$ . The structure function contains the discrete coher-

ent singly scattered information available in the raw diffraction intensity data. It is defined according to[37]

$$S(Q) = \frac{I_c(Q)}{N\langle f \rangle^2} - \frac{\langle (f - \langle f \rangle)^2 \rangle}{\langle f \rangle^2}, \quad (4)$$

which gives

$$\begin{aligned} S(Q) - 1 &= \frac{I_c(Q) - N\langle f^2 \rangle}{N\langle f \rangle^2} \\ &= \frac{I_d(Q)}{N\langle f \rangle^2}, \end{aligned} \quad (5)$$

where  $f$  is the  $Q$ -dependent x-ray scattering factor or  $Q$ -independent neutron scattering length as appropriate and  $\langle \dots \rangle$  represents an average over all atoms in the sample. In this equation,  $I_c(Q)$  is the coherent single-scattered intensity per atom and  $I_d(Q)$  is the discrete coherent scattering intensity, which excludes the self-scattering,  $N\langle f^2 \rangle$ . [37] The coherent scattering intensity is obtained from the measured intensity by removing parasitic scattering (e.g., from sample environments), incoherent and multiple scattering contributions and correcting for experimental effects such as absorption, detector efficiencies, detector dead-time and so on. [7] The resulting corrected measured intensity is normalized by the incident flux to obtain  $I_c(Q)$ . The self-scattering,  $N\langle f^2 \rangle$ , and normalization,  $N\langle f \rangle^2$ , terms are calculated from the known composition of the sample using tabulated values of  $f$ .

As evident in Eq. 4, to obtain  $S(Q) - 1$  from  $I_c(Q)$  we subtract the self-scattering,  $N\langle f^2 \rangle$ , which has no atom-pair correlation information, and divide by  $N\langle f \rangle^2$ . As a result,  $S(Q) - 1$  oscillates around zero, and asymptotically approaches it at high  $Q$  as the coherence of the scattering is lost. If the experimental effects are removed correctly, the resulting  $F(Q)$  and  $G(r)$  are directly related to, and can be calculated from, structural models. [37] The corrections are well controlled in most cases and refinements of structural models result in reduced  $\chi^2$  values that approach unity in the best cases. Some uncertainty in the corrections can be tolerated because they are mostly long-wavelength in nature (for example, the absorption correction), which results in aberrations

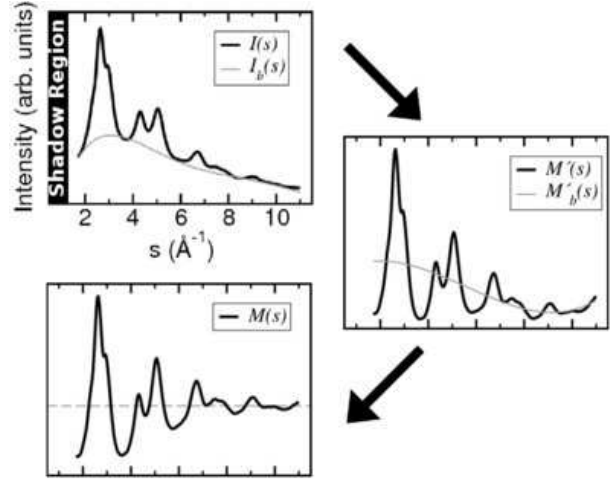


Figure 2: The UEC data reduction procedure showing the reduction of  $I(s)$  to  $M(s)$ .

in  $G(r)$  at very low- $r$  below any physically meaningful region of the PDF. [39]

## 4.2 UEC data reduction

In practice,  $M(s)$  is obtained from the raw experimental intensity,  $I(s)$ , by an empirical approach. [33] This approach is necessary because the reflection geometry employed to effectively sample the surface-dispersed nanoparticles results in a shadowing effect, i.e. the diffraction intensities collected at small exit angles are strongly attenuated due to surface absorption. In practice, due to the random nature of the surface roughness, the attenuation factor is not known precisely. It is not immediately clear that the empirical method results in quantitatively reliable mRDFs, as demonstrated in a more simple transmission geometry in which the tabulated atomic scattering form factor can be used directly to yield quantitative structure solutions of molecular systems. [27]

The UEC data reduction procedure is demonstrated in Fig. 2. First, an empirical background is estimated by fitting a slowly varying function, such as a low order polynomial, through the center or base of the raw intensity. This background is subtracted from the raw intensity. The background-subtracted

data are then divided by the same background function. We denote this estimated background as  $I_b(s)$  and can write the resulting intermediate intensity,  $M'(s)$ , as

$$M'(s) = \frac{I(s) - I_b(s)}{I_b(s)}. \quad (6)$$

The next step in processing the data is to adjust for any offset in the initial background. This secondary background,  $M'_b(s)$ , captures the slowly-varying components of  $M'(s)$ , and as a result the remaining signal oscillates around zero. The result is the molecular scattering intensity,

$$M(s) = M'(s) - M'_b(s). \quad (7)$$

### 4.3 Practical relationship between the molecular scattering and the total scattering structure function

In order to understand how  $M(s)$  relates to  $S(Q)$ , we consider an ideal case; scattering from a monatomic system with no undesirable experimental effects influencing the data. If measured without an offset,  $I_b$  captures only the slowly varying self-scattering from the (normalized coherent) scattering intensity. This self scattering is equal to  $N\langle f \rangle^2$  for a monatomic system. Thus,  $M'(s) = (I_c(s) - N\langle f^2 \rangle) / N\langle f \rangle^2 = I_d(s) / N\langle f \rangle^2 = S(s) - 1$ . Since this background is measured perfectly,  $M'_b = 0$ , and so  $M(s) = M'(s) = S(s) - 1$ .

In reality, the data are not ideal;  $I_b$  must correct for experimental effects, and  $M'_b$  must somehow compensate for the accuracy of  $I_b$ . More formally, we write the raw intensity as the coherent intensity modified by multiplicative term that captures multiplicative experimental effects (e.g., absorption correction) and an additive term representing the incoherent background and additive experimental effects (e.g., substrate scattering, inelastic scattering)

$$I(s) = \sigma(s)I_c(s) + \nu(s). \quad (8)$$

The background intensity,  $I_b(s)$ , estimates the modified self-scattering  $\sigma(s)N\langle f^2 \rangle$ , the incoherent scattering background, and the undesirable additive effects,  $\nu(s)$ . The goal in subtracting  $I_b(s)$  is to

remove the self-scattering and additive effects from the intensity. This background is typically estimated using a low-order polynomial, which can approximate the experimentally modified  $N\langle f^2 \rangle$  with relative accuracy.[40] The estimate is subject to error, however, which may be due to components of  $\nu(s)$  that are poorly estimated or due to an intentional offset of the estimated background curve. We denote this error by  $-\epsilon(s)$ . Thus, the first stage of the UEC data reduction results in

$$\begin{aligned} M'(s) &= \frac{\sigma(s)I_c(s) + \nu(s) - (\sigma(s)N\langle f^2 \rangle + \nu(s) - \epsilon(s))}{\sigma(s)N\langle f^2 \rangle + \nu(s) - \epsilon(s)} \\ &= \frac{\sigma(s)(I_c(s) - N\langle f^2 \rangle)}{\sigma(s)N\langle f^2 \rangle + \nu(s) - \epsilon(s)} \\ &\quad + \frac{\epsilon(s)}{\sigma(s)N\langle f^2 \rangle + \nu(s) - \epsilon(s)} \\ &= \frac{\sigma(s)(I_c(s) - N\langle f^2 \rangle)}{\sigma(s)N\langle f^2 \rangle + \nu(s) - \epsilon(s)} + \gamma(s). \end{aligned} \quad (9)$$

Note that  $\gamma(s)$  and the denominator in Eq. 9 are slowly varying functions of  $s$ .

The next step is to eliminate the effects of  $\gamma(s)$ , which result from the offset in the estimate of  $I_b(s)$ . Since  $\gamma(s)$  is slowly varying it can be fit with a low-order polynomial. With  $\gamma(s)$  eliminated, the result will oscillate around zero. There will be some error in this estimate as well, which we denote  $-\beta(s)$ . Thus,

$$M'_b(s) = \gamma(s) - \beta(s). \quad (10)$$

Using this expression for  $M'_b(s)$  gives

$$M(s) = \frac{\sigma(s)(I_c(s) - N\langle f^2 \rangle)}{\sigma(s)N\langle f^2 \rangle + \nu(s) - \epsilon(s)} + \beta(s). \quad (11)$$

This is very near to the form of Eq. 5. To get this in the desired form, we write  $I_c(s) - N\langle f^2 \rangle = (S(s) - 1)N\langle f \rangle^2$  (see Eq. 5) so that

$$M(s) = \alpha(s)(S(s) - 1) + \beta(s), \quad (12)$$

where

$$\alpha(s) = \frac{\sigma(s)N\langle f \rangle^2}{\sigma(s)N\langle f^2 \rangle + \nu(s) - \epsilon(s)}, \quad (13)$$

and we note that  $\alpha(s)$  is also slowly varying. Now, understanding the effective difference between  $M(s)$  and  $S(s) - 1$  reduces to understanding the effects  $\alpha(s)$  and  $\beta(s)$  have on the measured correlation function.

First we consider  $\beta(s)$ . By construction,  $\beta(s)$  is small, and contains only slowly varying components. As mentioned above, this means that  $\beta(s)$  contributes only to the low- $r$  region of the correlation function, below the physically interesting region.[39] If the experimental effects are not slowly varying, then the Fourier transform of  $\beta(s)$  will leak into the structurally relevant portion of the correlation function. The effect is unpredictable, but should be small.

The multiplicative term,  $\alpha(s)$ , is likely to have a more significant effect on the correlation function. In the best case,  $\alpha(s)$  is constant and it scales the peaks of the correlation function uniformly, which does not obscure the structural information. The only aspect of  $\alpha(s)$  that is controlled by the data reduction is how quickly it oscillates. This is controlled by how well the modified self-scattering is fit by the intensity background (manifest in  $\nu(s)$  and  $\epsilon(s)$ ). Depending on how well these factors are estimated,  $\alpha(s)$  may distort the peak profile of the correlation function. At worst, this could result in a measurable peak shift, which would complicate the extraction of reliable structure parameters.

## 5 Methods

Data have been collected on size-selected gold nanoparticles with diameter of approximately 20 Å using the UEC experimental setup described in §2. Further details on the sample preparation and data collection can be found elsewhere.[2] To gain quantitative information about the morphology of gold nanoparticles we modeled PDFs from experimental UEC data using three structure models: a 309-atom cuboctahedron (diameter 22.3 Å), a 309-atom Mackay icosahedron[41] (diameter 23.1 Å) and a 181-atom decahedron[42] (diameter 23.8 Å). These gold cluster types have been shown to exist at a similar size[43] and have been the subject of a previous UEC study.[33] We also fit these nanoparticle models with one fewer and one additional shell. The

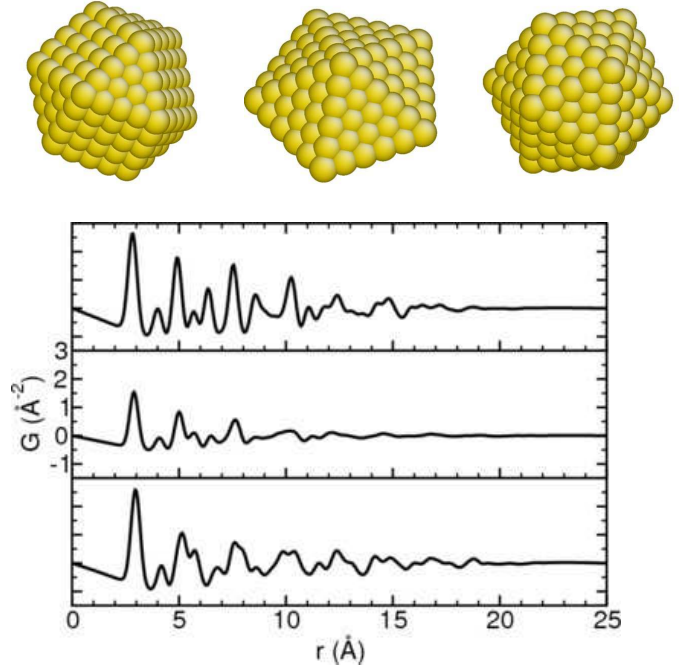


Figure 3: PDFs from likely models for  $\sim 20$  Å gold nanoparticles. Top: Cuboctahedral, decahedral and icosahedral models. Bottom: PDFs calculated from the cuboctahedral (top), decahedral (middle) and icosahedral (bottom) models.

results in those fits were considerably worse than for these nanoparticle sizes, and will not be reported.

The structure models are shown in Fig. 3 along with the theoretical PDF from each model.<sup>1</sup> As can be seen in that figure, the models give PDFs that are very different past 5 Å, which reflects their topographical differences. All nanoparticles were modeled with rigid atomic arrangements and uniform isotropic atomic displacement parameters (ADPs).

In all refinements the nanoparticle models were allowed to expand or contract isotropically keeping the number and relative positions of atoms in each model fixed. The samples are nominally mono-disperse, so to avoid complicating the analysis we have not attempted to model size distributions. Furthermore,

<sup>1</sup>Figures created with the AtomEye structure viewer.[44]

we have not considered strain effects besides a simple isotropic expansion of the models.

We calculate  $F(Q)$  from a structure model using the Debye equation,[45, 14] modified such that the pair-contributions are attenuated by a Debye-Waller factor, and this is transformed to  $G(r)$  according to Eq. 2. The Debye-Waller factor is derived from the ADPs and a refinable vibrational correlation term.[46, 47] A scale factor was refined to account for the undetermined scale of the raw intensity. Resolution factors[48] that broaden and dampen the PDF peaks were also refined to simulate the effects of the finite  $s$ -resolution of the measurement. The refinements were performed using a home-written least squares regression algorithm based on the PDFFIT2 program.[14]

We distinguish the fits by their agreement with the data. This is quantified with the weighted residual of the PDF, defined as

$$R_w = \sqrt{\frac{\sum_i \omega(r_i)(G(r_i) - G_m(r_i))^2}{\sum_i \omega(r_i)G(r_i)^2}}, \quad (14)$$

where  $G$  denotes the experimental PDF and  $G_m$  is the PDF calculated from a structure model. For this study the weights  $\omega(r_i)$  are equal for every point and therefore cancel in  $R_w$ . The  $R_w$  factor was calculated only over the physical portion of the fit range, which we estimate to be between 2.2 and 20 Å.

To test the robustness of the data reduction and refinement procedure, we have also performed refinements on the PDF produced from four different data reduction protocols and compared the results. These protocols differ in how the intensity background,  $I_b(s)$ , is determined. The different protocols produce different  $s$ -dependent scaling factors,  $\alpha(s)$ , and ultimately different PDFs. For two reduction procedures,  $I_b(s)$  is determined by fitting along the bottom of  $I(s)$  using 4th and 5th degree polynomials (denoted *poly4b* and *poly5b*, respectively), the latter of which is the standard procedure. [1] The other two procedures fit  $I_b(s)$  through the center of  $I(s)$  using a 7th degree polynomial (denoted *poly7c*) and an exponential function of the form  $\sqrt{s - s_0} \exp(-s^{0.75})$  (denoted *expn*) that is empirically found to well describe the shadowing effect and decay of the scatter-

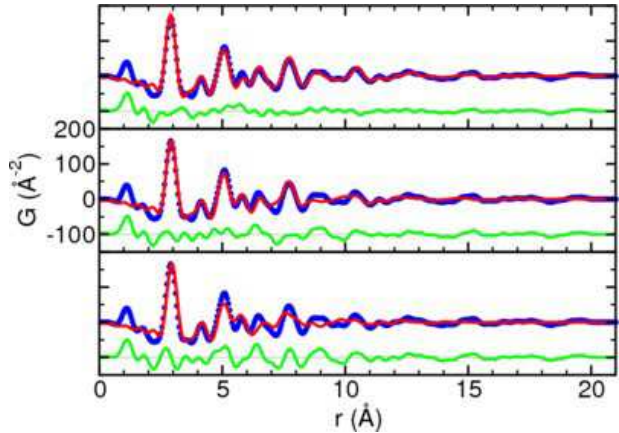


Figure 4: Fits to the standard data. *poly5b* data (blue dots), fit (red line) and difference (green line, offset). (Top) Cuboctahedral model. (Middle) Decahedral model. (Bottom) Icosahedral model. Note the comparative quality of the cuboctahedral fit above 5 Å and generally poor fit to the third and fourth peaks.

ing signal.

## 6 Results

### 6.1 Quantitative Structure Modeling

To determine whether the UEC data are of sufficient quality to differentiate, quantitatively, between structural models, we fit cuboctahedral, decahedral and icosahedral nanoparticle models to UEC PDF data produced using the standard procedure (*poly5b*) as described in §5.

Among the models used in these refinements, the cuboctahedral model stands out as the best, resulting in a  $R_w$  value of 0.23, compared to 0.30 for the decahedral model and 0.41 for the icosahedral model. These fits are shown in Fig. 4. None of the structure models reproduce the third and fourth peaks of the PDF well. It is possible that this misfit is due to errors introduced during the data reduction. We explore this possibility below. The structural results from the cuboctahedral model are shown in Table 1.

## 6.2 Robustness

Given the empirical nature of the methods for producing the PDF from the diffraction intensity, it is worthwhile to investigate the robustness of refinement results based on the different procedures. This will give insight into the influence of the data reduction procedure on the PDF, and will give us a quantitative measure of the systematic bias that may be introduced during data reduction. We have performed refinements of the cuboctahedral model described above to the PDF produced from the four different data reduction procedures described in §5 and demonstrated in Fig. 5.

As can be seen in Fig. 5, the data reduction procedures all produce  $sM(s)$  and PDF curves similar to each other. The major features of these curves (indicated by the dashed lines in the figure) are preserved using each procedure. The largest differences among the PDFs appear in the peak widths and amplitude ratios. Peak asymmetry is hard to detect given that the PDF sits on a negative baseline, and the peaks are therefore not Gaussian. The bottom panel of Fig. 5 shows the difference between the PDF from the *poly5b* background (the standard procedure) and the other PDFs, scaled so that the heights of the first peaks are identical. The pre-peak signal is rather different in each signal, indicative of the additive errors,  $\beta(s)$ , in  $sM(s)$  resulting from the data reduction procedures.

Fits to the data were performed using the cuboctahedral model as described in §5. The cuboctahedral model fits can be seen in Fig. 6 and are summarized in Table 1. In the table,  $a$  is the effective FCC lattice constant derived from the interior nearest neighbor distance. As seen from the figure and table, all fits are of variable quality, with a markedly improved  $R_w$  value for the exponential background. It can be seen that this fit reproduces the fourth peak significantly better than the other fits.

From Table 1 we see that the measured peak width parameter ( $U_{iso}$ ) is not robust with respect to the data reduction procedure. This indicates that the at least some of the data suffer from peak profile distortions due to the data reduction protocol. Considering the ideal data reduction scenario discussed

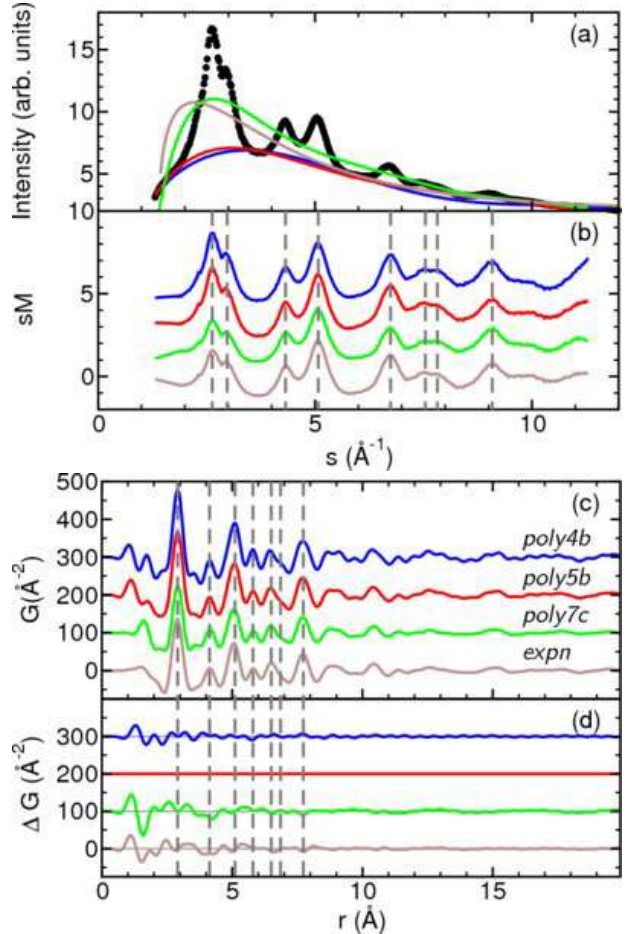


Figure 5: Similarity between structure functions from various data reduction procedures. Blue line: *poly4b*. Red line: *poly5b*. Green line: *poly7c*. Brown line: *expn*. See text. Note the similarity of the major profile features, as indicated by the dashed lines. (a)  $I_b(s)$  for each protocol through the raw intensity (black circles). (b)  $sM(s)$  for different reductions. (c) PDFs from the different reductions. (d) PDF differences taken from the *poly5b* PDF. All PDFs are scaled to have the same first-peak amplitude. The structural region is  $r > 2.2 \text{ \AA}$ .

Table 1: Refinement parameters from cuboctahedral fits. Here,  $a$  is the effective lattice parameter derived from nearest neighbor distances and  $U_{iso}$  is the isotropic ADP (see text). No standard deviations are shown on the refined parameters as we don't know uncertainties reliably on the raw intensities.

	$R_w$	$a(\text{\AA})$	$U_{iso}(\text{\AA}^2)$
<i>poly4b</i>	0.27	4.117	0.0250
<i>poly5b</i>	0.21	4.115	0.0264
<i>poly7c</i>	0.20	4.116	0.0167
<i>expn</i>	0.20	4.116	0.0185

in §4.3, where the ideal intensity background perfectly matches the modified self-scattering through the center of the raw intensity, we believe that protocols *poly7c* and *expn*, which estimate the background through the center of the raw intensity, introduce less error into the correlation function. This conclusion is supported by the superior low- $r$  fit agreement to these data and the smaller fit residuals ( $R_w$ ).

The effective lattice constant ( $a$ ) from Table 1 is robust with respect to the data reduction procedure. This shows that the errors in the correlation function introduced by the data reduction procedures are not severe enough to result in a measurable peak shift. Thus, the geometric structure information is readily accessible from the UEC data despite the uncontrolled aspects of the data reduction protocol.

We note that the estimated lattice parameter is smaller than that for bulk gold. This is not a physical effect, or a result of the data reduction protocol, but rather due to a lack of instrument calibration. Driven primarily by the interests of differential structural changes, UEC frequently treats the data using the known ground state structure as the reference. In the case where the ground state structure is not known, only relative changes can be obtained. Given the very small uncertainty of the refined lattice parameters shown here, these ground state data could be used to calibrate the UEC setup by comparing to data from the same particles measured with x-rays in a conventional PDF measurement, thus making the absolute structural solution from UEC possible.

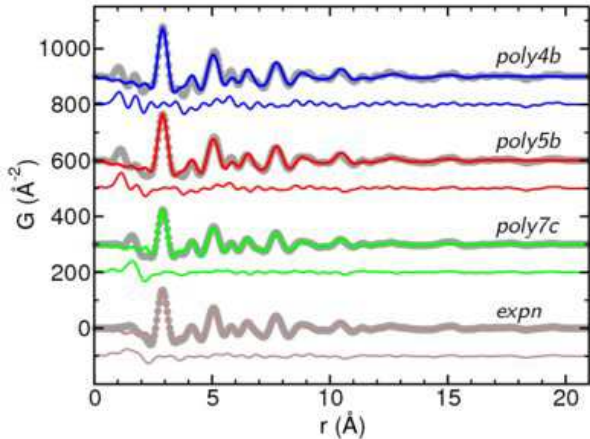


Figure 6: Fits using the cuboctahedral model to PDFs produced with different data reduction protocols. (See Fig. 5 for color key.) PDF fits (solid lines), data (gray circles) and difference between data and fit (solid lines, offset below).

## 7 Conclusions

We have shown the equivalence of the mRDF commonly used in UEC and the PDF typically employed in x-ray and neutron powder diffraction. This has allowed us to use powder diffraction modeling techniques to refine cuboctahedral, icosahedral and decahedral models to the PDF derived from UEC data. We have found that the cuboctahedral model agrees best with the data. This demonstrates that UEC data can be of sufficient quality to differentiate between different nanoparticle structure models.

We have tested the cuboctahedral model with multiple PDFs produced using different data reduction protocols that differ in how the intensity background is removed and the data normalized. Given the large differences in the background curves fit through the raw intensity data, we are able to determine the effective lattice parameter of the cuboctahedral model with remarkable certainty. We cannot determine with certainty the thermal displacement parameter within the model because this parameter is strongly influenced by the form of the intensity background.

The figure of merit of our best fits (cuboctahe-

dral *poly7c* and *expn*,  $R_w = 0.20$ ) is comparable to results from high-quality nanoparticle x-ray PDF studies.[25, 49] The cuboctahedral model affords little flexibility to compensate for systematic errors, so the results indicate that these errors are not significantly worse than what one would expect from synchrotron x-ray data. We conclude that, with careful data reduction and a standard system for calibration, UEC is applicable as a quantitative nanostructure probe.

## 8 Acknowledgments

This work was supported by the US National Science foundation through Grant DMR-0703940.

## References

- [1] Ruan, C.-Y., Vigliotti, F., Lobastov, V. A., Chen, S. Y., and Zewail, A. H. (2004) *Proc. Natl. Acad. Sci. USA* **101**, 1123.
- [2] Ruan, C.-Y., Murooka, Y., Raman, R., and Murdick, R. (2007) *Nano Lett.* **7**(5), 1290–1296.
- [3] Zewail, A. H. (2000) *J. Phys. Chem. A* **104**, 5660.
- [4] Zewail, A. H. (2006) *Annu. Rev. Phys. Chem.* **57**, 65.
- [5] Dwyer, J. R., Hebeisen, C. T., Ernstorfer, R., Harb, M., Deyirmenjian, V. B., Jordan, R. E., and Miller, R. J. D. (2006) *Phil. Trans. R. Soc. A* **364**, 741.
- [6] Robert E. Dinnebier and Simon J. L. Billinge, (ed.) (2008) *Powder diffraction: theory and practice*, Royal Society of Chemistry, London, England.
- [7] Egami, T. and Billinge, S. J. L. (2003) *Underneath the Bragg peaks: structural analysis of complex materials*, Pergamon Press, Elsevier, Oxford, England.
- [8] Gembicky, M. and Coppens, P. Jan 2007 *J. Synchrotron Radiat.* **14**(1), 133–137.
- [9] T. E. Weirich, Janos L. Lábár, and Xiaodong Zuo, (ed.) *Electron Crystallography: Novel approaches for structure determination of nano-sized materials* Amsterdam (2006) Springer.
- [10] Own, C. S., Marks, L. D., and Sinkler, W. Nov 2006 *Acta Crystallogr. A* **62**(6), 434–443.
- [11] Billinge, S. J. L. and Levin, I. (2007) *Science* **316**, 561–565.
- [12] Juhás, P., Cherba, D. M., Duxbury, P. M., Punch, W. F., and Billinge, S. J. L. (2006) *Nature* **440**(7084), 655–658.
- [13] Proffen, T. and Billinge, S. J. L. (1999) *J. Appl. Crystallogr.* **32**, 572–575.
- [14] Farrow, C. L., Juhás, P., Liu, J. W., Bryndin, D., Božin, E. S., Bloch, J., Proffen, T., and Billinge, S. J. L. (2007) *J. Phys: Condens. Mat.* **19**, 335219.
- [15] Tucker, M. G., Keen, D. A., Dove, M. T., Goodwin, A. L., and Hui, Q. (2007) *J. Phys.: Condens. Mat.* **19**, 335218.
- [16] Iwasaki, M., Fritsch, F. N., and Hedberg, K. (1964) *Acta Crystallogr.* **17**, 533.
- [17] Weirich, T., Ramlau, R., Simon, A., Hovmoller, S., and Zou, X. (1996) *Nature* **382**, 144.
- [18] Wagner, P., Terasaki, O., Ritsch, S., Nery, J., Zones, S., Davis, M., and Hiraga, K. (1999) *J. Phys. Chem. B* **103**, 8245.
- [19] Moss, B. and Dorset, D. (1982) *J. Polym. Sci. Pol. Phys.* **20**, 1789.
- [20] Wu, J. and Spence, J. (2002) *Acta Crystallogr. A* **58**, 580.
- [21] Huang, W. J., Sun, R., Tao, J., Menard, L. D., Nuzzo, R. G., and Zuo, J. M. (2008) *Nature Mater.* **7**(4), 308–313.

- [22] Dorset, D. (1995) Structural electron crystallography, Plenum Press, New York.
- [23] McGreevy, R. L. (2001) *J. Phys.: Condens. Mat.* **13(46)**, R877–R913.
- [24] Tucker, M. G., Dove, M. T., and Keen, D. A. (2001) *J. Appl. Crystallogr.* **34**, 630–638.
- [25] Masadeh, A. S., Božin, E. S., Farrow, C. L., Paglia, G., Juhás, P., Karkamkar, A., Kanatzidis, M. G., and Billinge, S. J. L. (2007) *Phys. Rev. B* **76**, 115413.
- [26] Neder, R. B. and Korsunskiy, V. I. (2005) *J. Phys.: Condens. Mat.* **17(5)**, S125–S134.
- [27] Srinivasan, R., Lobastov, V. A., Ruan, C.-Y., and Zewail, A. H. (2003) *Helv. Chim. Acta* **86**, 1763.
- [28] Ruan, C.-Y., Lobastov, V. A., Srinivasan, R., Goodson, B. M., Ihee, H., and Zewail, A. H. (2001) *Proc. Natl. Acad. Sci. USA* **98**, 7117.
- [29] Srinivasan, R., Feenstra, J. S., Park, S. T., Xu, S., and Zewail, A. H. (2005) *Science* **307**, 558.
- [30] Ruan, C.-Y., Lobastov, V. A., Vigliotti, F., Chen, S., and Zewail, A. H. (2004) *Science* **304**, 5667.
- [31] Baum, P., Yang, D.-S., and Zewail, A. H. (2007) *Science* **318**, 788.
- [32] Gedik, N., Yang, D.-S., Logvenov, G., Bozovic, I., and Zewail, A. H. (2007) *Science* **316**, 425.
- [33] Ruan, C.-Y., Murooka, Y., Raman, R. K., Murdick, R. A., Worhatch, R. J., and Pell, A. (2009) *Microsc. Microanal.* **15**, 323.
- [34] Raman, R. K., Murooka, Y., Ruan, C.-Y., Yang, T., Berber, S., and Tomanek, D. (2008) *Phys. Rev. Lett.* **101(7)**, 077401.
- [35] István Hargittai and Magdolna Hargittai, (ed.) (1988) Stereochemical applications of gas-phase electron diffraction, VHC Publishers, New York 1st edition.
- [36] Hedberg, K. and Iwasaki, M. (1964) *Acta Crystallogr.* **17**, 529.
- [37] Farrow, C. L. and Billinge, S. J. L. (2009) *Acta Crystallogr. A* **65(3)**, 232–239.
- [38] Warren, B. E. (1990) X-ray diffraction, Dover, New York.
- [39] Peterson, P. F., Gutmann, M., Proffen, T., and Billinge, S. J. L. (2000) *J. Appl. Crystallogr.* **33**, 1192–1192.
- [40] Doyle, P. A. and Turner, P. S. (1968) *Acta Crystallogr. A* **24(3)**, 390–397.
- [41] Mackay, A. L. (1962) *Acta Crystallogr.* **15**, 916–918.
- [42] Ino, S. (1966) *J. Phys. Soc. Jpn* **21(2)**, 346–362.
- [43] Cervellino, A., Giannini, C., and Guagliardi, A. (2003) *J. Appl. Crystallogr.* **36**, 1148–1158.
- [44] Li, J. (2003) *Model. Simul. Mater. Sc.* **11(2)**, 173–177.
- [45] Debye, P. (1915) *Annalen der Physik (Berlin, Germany)* **46**, 809–823.
- [46] I.-K. Jeong, Proffen, T., Mohiuddin-Jacobs, F., and Billinge, S. J. L. (1999) *J. Phys. Chem. A* **103**, 921–924.
- [47] Jeong, I. K., Heffner, R. H., Graf, M. J., and Billinge, S. J. L. (2003) *Phys. Rev. B* **67**, 104301.
- [48] Toby, B. H. and Egami, T. (1992) *Acta Crystallogr. A* **48(3)**, 336–46.
- [49] Gilbert, B. (2008) *J. Appl. Crystallogr.* **41**, 554.